Research Article

Jian-Qi Zhang, Jing-Xin Liu, Hui-Lai Zhang, Zhi-Rui Gong, Shuo Zhang, Lei-Lei Yan, Shi-Lei Su*, Hui Jing* and Mang Feng*

Topological optomechanical amplifier in synthetic $\mathcal{PT}$-symmetry

https://doi.org/10.1515/nanoph-2021-0721
Received November 17, 2021; accepted January 30, 2022; published online February 14, 2022

Abstract: We propose how to achieve synthetic $\mathcal{PT}$ symmetry in optomechanics without using any active medium. We find that harnessing the Stokes process in such a system can lead to the emergence of exceptional point (EP), i.e., the coalescing of both the eigenvalues and the eigenvectors of the system. By encircling the EP, both nonreciprocal optical amplification and chiral mode switching can be achieved. As a result, our synthetic $\mathcal{PT}$-symmetric optomechanics works as a topological optomechanical amplifier. This provides a surprisingly simplified route to realize $\mathcal{PT}$-symmetric optomechanics, indicating that a wide range of EP devices can be created and utilized for various applications such as topological optical engineering and nanomechanical processing or sensing.

Keywords: cavity optomechanics; chirality; topological amplification.

Jian-Qi Zhang and Jing-Xin Liu contributed equally to this work.

***Corresponding authors: Mang Feng**, State Key Laboratory of Magnetic Resonance and Atomic and Molecular Physics, Wuhan Institute of Physics and Mathematics, Innovation Academy of Precision Measurement Science and Technology, Chinese Academy of Sciences, Wuhan 430071, China; and School of Physics, Zhengzhou University, Zhengzhou 450001, China, E-mail: mangfeng@wipm.ac.cn;
Hui Jing, Key Laboratory of Low-Dimensional Quantum Structures and Quantum Control of Ministry of Education, Department of Physics and Synergetic Innovation Center for Quantum Effects and Applications, Hunan Normal University, Changsha 410081, China, E-mail: jinghui73@foxmail.com. https://orcid.org/0000-0001-5091-2057; and **Shi-Lei Su**, School of Physics, Zhengzhou University, Zhengzhou 450001, China, E-mail: slsu@zzu.edu.cn. https://orcid.org/0000-0002-2153-5827
Jian-Qi Zhang, State Key Laboratory of Magnetic Resonance and Atomic and Molecular Physics, Wuhan Institute of Physics and Mathematics, Innovation Academy of Precision Measurement Science and Technology, Chinese Academy of Sciences, Wuhan 430071, China. https://orcid.org/0000-0001-5264-8560
Jing-Xin Liu, State Key Laboratory of Magnetic Resonance and Atomic and Molecular Physics, Wuhan Institute of Physics and Mathematics, Innovation Academy of Precision Measurement Science and Technology, Chinese Academy of Sciences, Wuhan 430071, China; School of Physics, Zhengzhou University, Zhengzhou 450001, China; and National Laboratory of Solid State Microstructures, School of Physics, Nanjing University, Nanjing 210093, China
Hui-Lai Zhang, Key Laboratory of Low-Dimensional Quantum Structures and Quantum Control of Ministry of Education, Department of Physics and Synergetic Innovation Center for Quantum Effects and Applications, Hunan Normal University, Changsha 410081, China
Zhi-Rui Gong, The College of Physics and Optoelectronic Engineering, Shenzhen University, Shenzhen 518060, China
Shuo Zhang, Henan Key Laboratory of Quantum Information and Cryptography, Zhengzhou, 450001, China
Lei-Lei Yan, School of Physics, Zhengzhou University, Zhengzhou 450001, China

1 Introduction

Unconventional effects of exceptional points (EPs), i.e., non-Hermitian spectral degeneracies at which the eigenvalues and their eigenvectors coalesce, as revealed in recent years [1–26], have radically changed our understanding of complex systems and led to important applications. Novel EP devices have been fabricated and utilized for realizing, e.g., ultra-sensitive metrology [27–30], single-mode lasing [31–34], loss-induced transparency [35, 36], and wireless power transfer [37, 38]. In particular, EP-enabled exotic topological effects have attracted intense interests [39–43], such as non-Hermitian skin effect [43–46], topological energy transfer [47, 48], and asymmetric mode switching [49–56], providing new opportunities for such a wide range of fields as synthetic photonics and topological physics [59–61]. However, due to the accumulation of dissipations in topological operations, as far as we know, topological amplifier which works as a key element in practical application has remained a challenge as topological EP devices till now.

In this work, we propose how to achieve synthetic $\mathcal{PT}$ symmetry and topological amplifier in optomechanics [57, 58, 62], without the need of any active medium. We find that the optomechanical Stokes processes can be harnessed to compensate the optical losses and thus realize

$\mathcal{PT}$ symmetry in such a passive system [34, 63] without complexities, such as fabricating gain materials in active systems [1, 12, 64]. As another merit, topological optical amplifications can be realized here by simply tuning the optical modes rather than steering the acoustic modes [47] or designing materials with modulated structures [48–56]. Our work confirms that optomechanical systems can serve as a powerful tool to observe and utilize various topological EP effects.

In comparison with the previous works for the EP, our scheme owns significant differences as follows. First of all, in our work there exists an optical gain with a tunable center frequency as the special character of cavity optomechanics via a tunable frequency of the pump field. It is beyond the traditional gain processes, especially for the one in cavity optomechanics [34], where the center frequency of gain cannot be tuned for the certain frequency of the pump field. Secondly, different from the previous works for topological energy transfer in waveguides [48–56] or optomechanical phonon modes [47], which are limited by the accumulation of dissipations, our work illustrates that the dissipation accumulation can be overcome by employing the time-dependent gain with a tunable center frequency from the Stokes processes. Thirdly, contrary to the path-dependent topological dynamics with waveguides, where these fabricated optical systems lose their tunability, our optical system is time-dependent, and thus feasible to simulate the topological dynamics with different trajectories and topological properties. Finally, different from the previous work for energy transfer [47], where the effective two-level structure of phonon modes limits its application on the topological amplifier, our system benefits from the configuration of micro-toroidal resonators. This configuration leads to forward and backward transmissions taking different physical dynamics, and enables our system to work as a topological amplifier.

2 Synthetic $\mathcal{PT}$ symmetric optomechanics

We start by considering a passive optomechanical system as shown in Figure 1(a), where a micro-toroidal optomechanical resonator (MOR) evanescently couples to a passive micro-toroid resonator (PMR) [34, 63]. This system can be described in the simplest level by the Hamiltonian

$$H = \frac{p^2}{2m} + \frac{1}{2}m\omega_m^2 q^2 - \chi q a_{\circlearrowleft}^{\dagger} a_{\circlearrowleft} + H_c, \tag{1}$$

where q and p are position and momentum operators of the vibrational mode, respectively. The vibrational mode takes

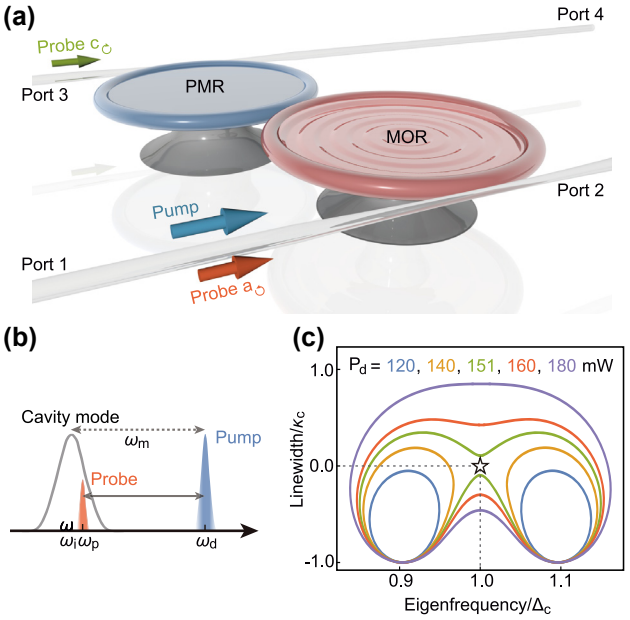

Figure 1: Synthetic $\mathcal{PT}$ symmetry in a passive optomechanical system without gain materials. (a) Two resonators, denoted by MOR and PMR, are evanescently coupled with each other and also coupled with optical fibers. A blue-detuned pump is input at the port 1 and the probe field enters from the ports 1 and 3. (b) In the propagation direction of the pump, the low-frequency probe acquires an effective gain from the pump via the Stokes process. (c) The eigenfrequency Re [ω] and its linewidth Im [ω] are the functions of the detuning Ω for different values of the pump power P_d.

an effective mass m and an eigenfrequency ω_m. The optical mode $a_{\circlearrowleft}$ in MOR couples to the vibrational mode via a radiation pressure coupling χ. Optical mode $a_{\circlearrowleft}$ is counter clockwise at frequency ω_a, which is driven (detected) by a pump (probe) field with frequency ω_d (ω_p) and amplitude $\sqrt{2\kappa_a}s_d$ ($\sqrt{2\kappa_a}s_{a_{\circlearrowleft}}$) from input port 1, while the optical mode $c_{\circlearrowleft}$ of PMR in clockwise at frequency ω_c is only detected by a probe field with frequency ω_p and amplitude $\sqrt{2\kappa_c}s_{c_{\circlearrowleft}}$ from input port 3. In the rotating frame at frequency ω_d, the Hamiltonian for the cavities is given by

$$\begin{aligned} H_c/\hbar = {} & \Delta_a a_{\circlearrowleft}^{\dagger} a_{\circlearrowleft} + \Delta_c c_{\circlearrowleft}^{\dagger} c_{\circlearrowleft} + g\left(a_{\circlearrowleft}^{\dagger} c_{\circlearrowleft} + \text{H.c.}\right) \\ & + i\sqrt{2\kappa_a}s_d\left(a_{\circlearrowleft}^{\dagger} - a_{\circlearrowleft}\right) \\ & + i\sqrt{2\kappa_a}s_{a_{\circlearrowleft}}\left(a_{\circlearrowleft}^{\dagger} e^{-i\Omega t} - \text{H.c.}\right) \\ & + i\sqrt{2\kappa_c}s_{c_{\circlearrowleft}}\left(c_{\circlearrowleft}^{\dagger} e^{-i\Omega t} - \text{H.c.}\right), \end{aligned} \tag{2}$$

where $a_{\circlearrowleft}$ $\left(a_{\circlearrowleft}^{\dagger}\right)$ and $c_{\circlearrowleft}$ $\left(c_{\circlearrowleft}^{\dagger}\right)$ are the annihilation (creation) operators of MOR and PMR, respectively. $\Omega = \omega_p - \omega_d$ ($\Delta_{i=a,c} = \omega_i - \omega_d$) is the detuning between the fixed

probe field (cavity modes) and the tunable pump field. g is the evanescent coupling between MOR and PMR. $s_{\rm i} = \sqrt{P_{\rm i}/\hbar\omega_{\rm i}}$ is governed by power $P_{\rm i}$ for ${\rm i} = {\rm p}, a_{\circlearrowleft}, c_{\circlearrowright}$, and $\kappa_{\rm a(c)}$ is the decay rate for mode $a_{\circlearrowleft}$ ($c_{\circlearrowleft}$).

In the blue-sideband regime ($\Omega \simeq -\omega_m$), by employing the mean-value equations for Hamiltonian (1) and eliminating the vibrational mode, we obtain the effective mean-value equations for optical modes in the frequency domain as [65, 66]

$$\begin{aligned} -i\Omega a_{\circlearrowleft} &= -(\kappa_{\rm eff} + i\Delta_{\rm eff})a_{\circlearrowleft} - igc_{\circlearrowright} + \sqrt{2\kappa_{\rm a}}s_{a_{\circlearrowleft}}, \\ -i\Omega c_{\circlearrowright} &= -(\kappa_{\rm c} + i\Delta_{\rm c})c_{\circlearrowright} - iga_{\circlearrowleft} + \sqrt{2\kappa_{\rm c}}s_{c_{\circlearrowright}}, \end{aligned} \tag{3}$$

where the effective detuning and gain are, respectively,

$$\Delta_{\rm eff} = \beta\omega_m \sin\theta/|\Omega_m| + \Delta_{\rm a} - \chi q_{\rm s}/\hbar \tag{4}$$

and

$$\kappa_{\rm eff} = \kappa_{\rm a} - \beta\omega_m \cos\theta/|\Omega_m| \tag{5}$$

with $\Omega_m = \gamma_m/2 - i(\Omega + \omega_m)$, $\beta = \chi q_{\rm s}/(2\hbar)$, $e^{i\theta} = \Omega_m/|\Omega_m|$, and $q_{\rm s}$ being the steady-state position [65]. The effective detuning $\Delta_{\rm eff}$ can be adjusted by mean photon number via the optomechanical interaction. As sketched in Figure 1(b), the Stokes photons are created at frequency $\omega_{\rm p} \simeq \omega_{\rm d} - \omega_m$ by emitting phonons at frequency ω_m, resulting in an effective gain $\kappa_{\rm eff}$ for the probe field. This provides a natural way to reach the gain–loss balance or $\mathcal{PT}$ symmetry, which is fundamentally different from the previous works using active materials [31–33], tunable dissipation in passive cavities [34], and modulated structures [48–56].

In the adiabatic limit, the non-Hermitian Hamiltonian of optical modes $a_{\circlearrowleft}$ and $c_{\circlearrowright}$ for Eq. (3) can be written in a time-dependent manner [12, 65]

$$H_{\rm eff}(t) = \begin{pmatrix} \Delta_{\rm eff}(t) - i\kappa_{\rm eff}(t) & g \\ g & \Delta_{\rm c} - i\kappa_{\rm c} \end{pmatrix}, \tag{6}$$

which has the eigenmodes

$$|\psi_{\pm}(t)\rangle = (-i\lambda(t) \pm \sqrt{1-\lambda(t)^2})\,|a_{\circlearrowleft}\rangle + |c_{\circlearrowright}\rangle, \tag{7}$$

and the eigenvalues

$$\omega = \omega_{\pm} = V(t)/2 \pm g\sqrt{1-\lambda(t)^2}. \tag{8}$$

Here

$$V(t) = \Delta_{\rm eff} + \Delta_{\rm c} - i(\kappa_{\rm eff} + \kappa_{\rm c}), \tag{9}$$

and

$$\lambda(t) = \left[\kappa_{\rm eff}(t) - \kappa_{\rm c} + i(\Delta_{\rm eff}(t) - \Delta_{\rm c})\right]/2g. \tag{10}$$

$|a_{\circlearrowleft}\rangle$ and $|c_{\circlearrowright}\rangle$ denote optical modes $a_{\circlearrowleft}$ and $c_{\circlearrowright}$, respectively.

The topological features of Hamiltonian (6) can be identified from the complex eigenvalues (8) versus detuning Ω with different pump power $P_{\rm d}$ as plotted in Figure 1(c). Two independent orange circles ($P_{\rm d} = 140\,{\rm mW}$) are gradually melting into a big green circle ($P_{\rm d} = 151\,{\rm mW}$) with the increase of the pump power $P_{\rm d}$. It is the larger pump power $P_{\rm d}$ that provides a larger effective gain and ensures the EP to be enclosed in closed circles. In addition, topological features can also be identified from the Riemann surface in Figure 2.

3 Topological engineering around EPs

To describe the topological dynamics around the EP, we need to acquire the effective scattering matrix of Hamiltonian (6) at first.

We assume an evolution trajectory consisting of N short sections, where the scattering matrix regarding the section k is given by

$$\begin{aligned} U_k^{\rm eff} = {} & \exp[-i(\delta\Delta/2 - i\delta\kappa/2)T_0] \\ & * \begin{pmatrix} \cos\dfrac{\lambda T_0}{2} - \eta\sin\dfrac{\lambda T_0}{2} & -\dfrac{2ig}{\lambda}\sin\dfrac{\lambda T_0}{2} \\ -\dfrac{2ig}{\lambda}\sin\dfrac{\lambda T_0}{2} & \cos\dfrac{\lambda T_0}{2} + \eta\sin\dfrac{\lambda T_0}{2} \end{pmatrix} \end{aligned} \tag{11}$$

with

$$\begin{cases} \lambda = \sqrt{4g^2 + (\delta\Delta - i\delta\kappa)^2}, \\ \eta = \dfrac{i\delta\Delta + \delta\kappa}{\lambda}, \\ \delta\Delta = \Delta_{\rm eff}[(k-1)T_0] - \Delta_{\rm c}, \\ \delta\kappa = \kappa_{\rm eff}[(k-1)T_0] - \kappa_{\rm c}, \end{cases} \tag{12}$$

where T_0 is the evolution time for each section.

The corresponding total scattering matrix can be written as

$$U = \Pi_{k=1}^{N} U_k^{\rm eff}, \tag{13}$$

which shows that the amplification of the transmission field is determined by the time-dependent net gain $\delta\kappa$ via the Stokes processes, and the time-dependent evolution mode $|\psi(t)\rangle$ can be expressed as

$$|\psi(t)\rangle = U|\psi(t=0)\rangle, \tag{14}$$

with an initial mode $|\psi(t=0)\rangle$ for the time $t = 0$.

Next, to illustrate the NATs in the topological dynamics of our system, we simulate the evolution trajectories for topological operations in counter-clockwise (CCW) and

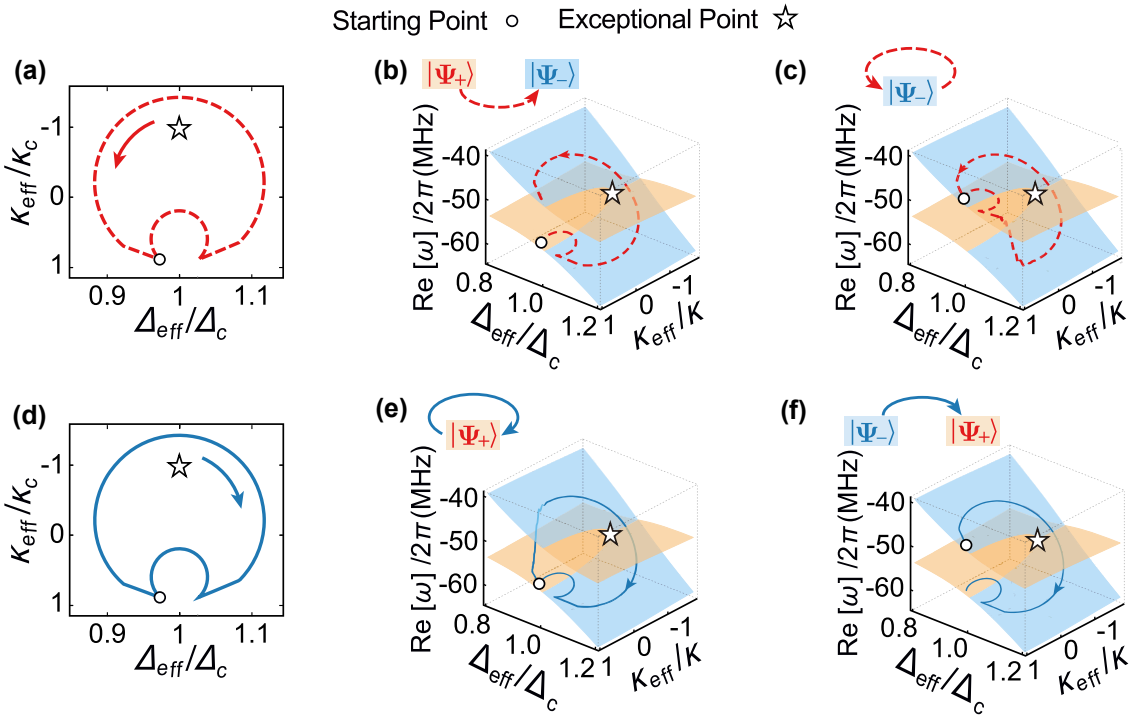

Figure 2: Energy dynamics Re [ω] and their trajectories with chirality follow the loops of topological operations with EP. (a and d) Loops of the topological operation, where the topological trajectories start from the initial eigenmodes plotted in the following panels. (b and e) Initial eigenmode $|\psi_+(t=0)\rangle$ and (c and f) initial eigenmode $|\psi_-(t=0)\rangle$ in the parameter spaces of the eigenenergy Re [ω], effective detuning Δ_{eff} and decay rate κ_{eff}. Arcs with arrows represent the topological operation directions in CCW (dashed red) and CW (solid blue). Here, eigenenergies for eigenmodes $|\psi_+\rangle$ and $|\psi_-\rangle$ are plotted in orange and blue. Parameters for simulations are $T = 0.01$ ms, $\omega_m/2\pi = 51.8$ MHz, $\gamma_m/2\pi = 41$ kHz, $m = 20$ ng, $\Delta_c = -\omega_m$, $g/2\pi = 5$ MHz, $\kappa/2\pi = 5$ MHz, $\kappa_c = \kappa_a = \kappa$, $\lambda = 390$ nm, $\chi/2\pi = 12 \times 10^{18}\hbar$ [8, 34, 63, 68].

clockwise (CW) following the scattering matrix (13) with $N = 4000$ in Figure 2.

Figure 2 indicates some trajectories between two eigenenergy surfaces in the parameter space as shown in Figure 2(c and e). These trajectories from the unsteady eigenmode $|\psi_+\rangle$ to the steady one $|\psi_-\rangle$ are regarding NATs. The NATs will appear when the topological operation times is longer than the coherence times of the optical modes [67]. Therefore, NATs enable topology-dependent energy transfers and own chiral properties in the dynamical encircling of the EP in the parameter space.

More specifically, our system is dominated by loss ($|\kappa_{eff}| < \kappa$). When the high energy surface is in $|\psi_+\rangle$ ($\Delta_{eff} > \Delta_c$), the high energy eigenmode $|\psi_+\rangle$, following the topological operations in CCW [see Figure 2(a)], will decay to its steady eigenmode $|\psi_-\rangle$ as in Figure 2(c). That is a traditional transition regarding dissipations. In contrast, when high energy surface is in $|\psi_-\rangle$ ($\Delta_{eff} < \Delta_c$), the low energy eigenmode $|\psi_+\rangle$, following the topological operations in CW [see Figure 2(d)], will decay to the high energy eigenmode $|\psi_-\rangle$ as in Figure 2(e). That works as the counterintuitive NAT from the low energy surface to the high one. This counterintuitive transition, resulting from detuning ($\Delta_{eff} - \Delta_c < 0$), ensures the steady eigenmode with a higher eigenenergy as in Eq. (8).

The eigenenergy surface in Figure 2 also indicates that the EP of synthetic $\mathcal{PT}$ symmetric optomechanics can be induced by the effective gain from Stokes processes via radiation pressure coupling. This effective gain takes tunable frequency for the radiation pressure coupling. That is different from the traditional gain methods based on rare-earth-doped gain media [10, 28, 31–33] and stimulated Brillouin processes [17], where the effective gain is limited by the frequencies of optical modes and gain materials. Moreover, in comparison to the conventional ideas induced by the coupling strength [8, 9] and the loss [5, 36, 69], our system provides an alternative way to observe $\mathcal{PT}$-symmetric breaking with the effective gain.

To illustrate the nontrivial topological properties of our system, we have to introduce the topological number. Here, we can define the topological number as vorticity ν in Ref. [70].

According to Ref. [70], to show the topological invariant of the topological operations, we use the invariant vorticity ν for eigenenergies $\omega_{\pm}$ in the complex-energy plane as

$$\nu(\alpha) = -\frac{1}{2\pi}\oint_{\alpha} \nabla_k \arg[\omega_+(k) - \omega_-(k)]\mathrm{d}k,$$

where α is a closed loop in the complex-energy plane, and $k = \Omega$ ($k = P_d$) is for the fixed pump field P_d (detuning Ω). This equation shows that the EP is (is not) enclosed in the loops of the complex-energy plane for $\nu = \pm 0.5$ ($\nu = 0$). Then we can obtain the red dash curves and the solid blue one in Figure 2, corresponding to $\nu = 0.5$ and $\nu = -0.5$, respectively. In addition, it is worthy to point out that the topological feature can also be observed from the linewidth and eigenenergy of the eigenmodes in Figure 1(c), where two independent orange circles ($P_d = 140$ mW) for eigenmodes will melt into a big green curve ($P_d = 151$ mW) by increasing the pump power.

4 Numerical simulation and discussion

In this section, we demonstrate our synthetic $\mathcal{PT}$ symmetric system to work as a topological amplifier with numerical simulations.

4.1 Topological energy transfer

To illustrate topological energy transfer and its chiral properties, we plot the trajectories for the loops of topological operations enclosing an EP in CW and CCW as in Figure 2.

When the EP is enclosed in the loops of topological operations, we assume the topological operation time T to be long enough in accomplishment of a single NAT. In this case, topological trajectories for different initial eigenmodes depend on the topological operation direction and own chirality. For example, only the initial mode $|\psi_+(t=0)\rangle$ [$|\psi_-(t=0)\rangle$] evolving along the Riemann surface in CCW (CW) can be transferred to $|\psi_-(t=T)\rangle \simeq |\psi_+(t=0)\rangle$ as in Figure 2(b) [$|\psi_+(t=T)\rangle \simeq |\psi_-(t=0)\rangle$ as in Figure 2(f)]. Otherwise, the optical mode will return to its initial mode $|\psi_+(t=T)\rangle \simeq |\psi_+(t=0)\rangle$ as in Figure 2(c) [$|\psi_-(t=T)\rangle \simeq |\psi_-(t=0)\rangle$ as in Figure 2(e)] since the NAT process blocks the eigenmodes swapping along the Riemann surface. As a result, topological energy transfer between two optical modes can be achieved, taking the feature of chirality. The above topological energy transfer and chirality can also be understood from the combination of the unsteady and steady eigenmodes, similar to the results characterized experimentally [49, 50, 54–56]. Due to this reason, this chirality can be switched off by further increasing the topological operation time T [65], as predicted in Ref. [12].

4.2 Topological amplification

The topological energy transfer mentioned above inspires us to achieve time-dependent topological optomechanical amplification for optical probe pulses with tunable topological properties by designing loops enclosing EP with large enough gain in the parameter space. Therefore, we will use probe pulses to illustrate the time-dependent topological optomechanical amplification as follows.

To quantify the performance of time-dependent topological optomechanical amplification under the influence of the probe field frequency, we plot transmission spectra for probe pulses in Figure 3 with the scattering matrix (13) and experimentally achievable parameters [8, 34, 63, 68], which ensures the largest effective gain for simulation to be $\kappa_{\mathrm{eff}}/2\pi \simeq -7.1$ MHz [65] with the pump power $P_{\mathrm{d}} = 180$ mW. Then the features of tunability, chirality, and topology can be illustrated from the transmissions in the topological dynamics with and without the EP for different values of vorticity number ν [65, 70, 71] as elucidated below. In the following, we assume the input probe pulses at ports 1(2) and 3(4) are in forward transmission eigenmodes $|\psi_{\pm}(t=0)\rangle$ of the system [49, 50, 54–56].

When EP is not encircled by the trajectories of topological operations ($\nu = 0$), the topological operations can be accomplished within the coherence time in the adiabatic limit, as mentioned by the traditional adiabatic theory [66]. This means that our system can evolve along the eigenenergy surface $|\psi_{\pm}\rangle$ and return to its initial modes $|\psi_{\pm}(t=T)\rangle = |\psi_{\pm}(t=0)\rangle$ without the NAT processes (see Figure S5 in [65]). In other words, no chirality exists in the transmissions as in Figure 3(a), where all the transmission spectra for topological operations in CCW and CW share the same value $T_{mn} \leq -12$ dB since the loss dominates the system in this case.

On the other hand, when EP is enclosed by the trajectories of topological operations ($\nu = \pm 0.5$), the chiral amplification of the energy can be found from the spectra difference between the forward transmissions T_{+-} (T_{-+}) and T_{--} (T_{++}), which are input from ports \{1, 3\} and output at ports \{2, 4\}. Specifically, only the transmission T_{+-}

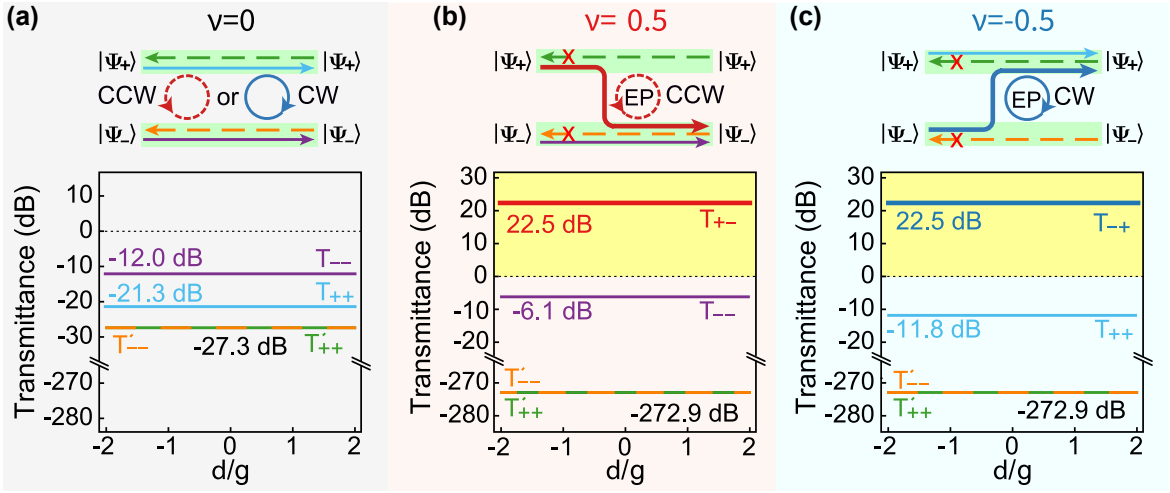

Figure 3: Transmission spectra T_{mn} from the input eigenmode of forward transmissions $|\psi_m(t=0)\rangle$ to the output eigenmode $|\psi_n(t=T)\rangle$ with $m,n=\pm$. Different topological dynamics is sorted via invariant vorticity ν. (a) Reciprocal transmission spectra T_{mn} for trival topological dynamics in CCW and CW ($\nu=0$) without the EP for the topological operation time of $T=0.1\,\mu$s with $\Delta_{\rm eff}/\Delta_{\rm c}\in\{0.9,0.92\}$ and $\kappa_{\rm eff}/\kappa_{\rm c}\in\{0.15,0.3\}$ [65]; (b and c) Non-reciprocal transmission spectra T_{mn} for nontrival topological dynamics encircling the EP in (b) CCW ($\nu=0.5$) and (c) CW ($\nu=-0.5$) with $T=1\,\mu$s, $\Delta_{\rm eff}/\Delta_{\rm c}\in\{0.9,1.1\}$ and $\kappa_{\rm eff}/\kappa_{\rm c}\in\{-1.2,0.3\}$ [65]. The transmission spectra are characterized with $T_{mn}=\langle\psi_m(t=0)|\psi_n(t=T)\rangle$. Detuning δ is the deviation frequency between the real probe pulses and the ideal ones at frequency $\omega_{\rm p}$, and vorticity number ν is a topological invariant [65, 70, 71]. The effective parameters satisfy the approximate conditions of the theoretical derivations in supplemental materials [65]. Other parameters take the same values as in Figure 2.

(T_{-+}) from the initial eigenmode $|\psi_+(t=0)\rangle$ ($|\psi_-(t=0)\rangle$) to the final eigenmode $|\psi_-(t=T)\rangle$ ($|\psi_+(t=T)\rangle$) in CCW (CW) can be amplified, as indicated by the solid lines in Figure 3(b and c). Otherwise, the transmission T_{--} (T_{++}) from the initial eigenmode $|\psi_-(t=0)\rangle$ ($|\psi_+(t=0)\rangle$) to the final eigenmode $|\psi_-(t=T)\rangle$ ($|\psi_+(t=T)\rangle$) in CCW (CW) will be suppressed by the NAT processes due to the combination of gain and loss, see the curves in Figure 2(c and e). That is to say, the chirality regarding the dynamical enclosing of an EP implies that the final eigenmodes are only determined by the directions of the topological operations in CCW and CW, and the amplification (suppression) of the initial modes depends on the directions of the topological operations, see red (dark blue) curves in Figure 3(b and c). Nevertheless, these amplifications would be less than the ones in numerical simulations for the limitation of saturation of Stokes processes [34], while the ratios of amplification of optical modes in output probe pulses will keep in a constant, since the output probe pulses are always the eigenmodes of the system.

According to the above discussion, our topological amplification ($\nu\neq0$) results from the accumulation of the gain and loss via NAT processes. The NAT processes lead to our topological amplification beyond the adiabatic condition. Therefore, the shortest time for our topological operation is the time to finish a single NAT, i.e., constrained by both the loss and the effective gain.

4.3 Robustness of the topological amplification

Now we will demonstrate the robustness of the topological amplification with different initial modes by simulating the fidelity of the final mode $|\psi(t=T)\rangle=|\psi_\pm\rangle$ with different initial mode $|\psi(t=0)\rangle=\cos\theta|c_{\circlearrowleft}\rangle+e^{i\phi}\sin\theta|a_{\circlearrowleft}\rangle$ in Figure 4.

Figure 4 shows, when topological operations do not contain an EP, the initial mode is the same as the final one. It is due to the adiabatic condition. It can be identified from the oscillations of fidelities (see dotted curves). In particular, this result can be easily followed when the initial mode is in $|a_{\circlearrowleft}\rangle$. In this case, the final mode is independent of the initial angle ϕ and takes a constant fidelity of 0.5 (see dotted curves in green). On the other hand, when the topological operations contain an EP, the final modes must be the eigenmodes (see solid lines). We can select the eigenmodes via the evolution directions in CCW and CW (see Section 4.2). These phenomena can also be understood as the robustness original from topological properties.

4.4 Topological amplifier

To show our system working as a topological amplifier, we have to demonstrate the above topological optomechanical amplification owning the feature of nonreciprocity. The backward transmissions, which are input from ports

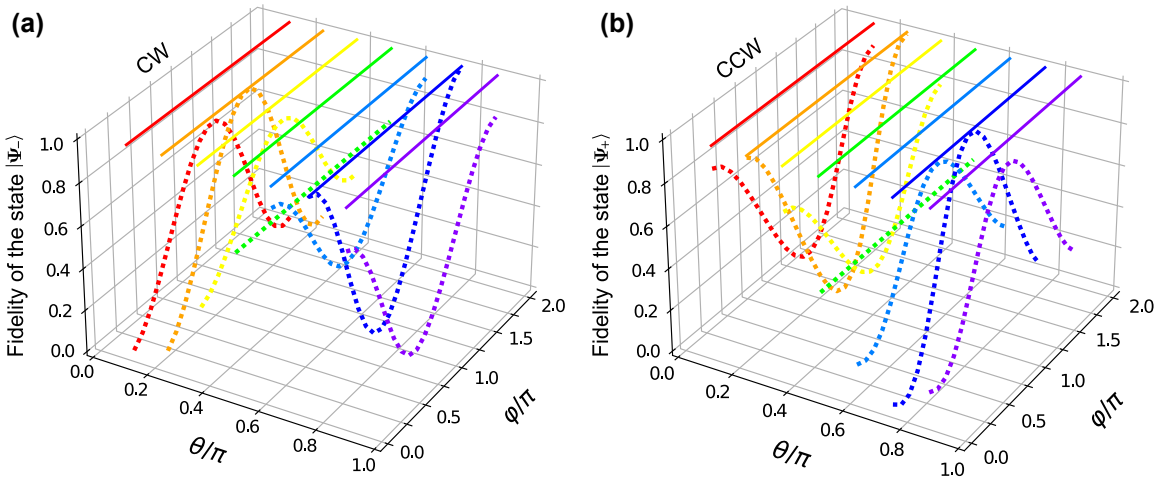

Figure 4: The fidelity of different topological operations in (a) CCW and (b) CW with different initial states. Here, solid lines represent topological amplification of the nontrival topological operations with an EP in (a) CCW ($\nu = 0.5$) and (b) CW ($\nu = -0.5$), while the dotted curves illustrate the trival topological operations without and EP in CCW and CW ($\nu = 0$). Parameters in the simulations are $\omega_m/2\pi = 51.8$ MHz, $\gamma_m/2\pi = 41$ kHz, $m = 20$ ng, $\Delta_c = -\omega_m$, $g/2\pi = 5$ MHz, $\kappa/2\pi = 5$ MHz, $\kappa_c = \kappa_a = \kappa$, $\lambda = 390$ nm, $\chi/2\pi = 12 \times 10^{18}\hbar$, and the topological operation times are $T = 10$ μs for (a and b) and $T = 4.1$ μs for (c and d). Other parameters take the same values as in Figure 2.

\{2, 4\} and output at ports \{1, 3\}, are denoted by the dashed lines in Figure 3(b and c) with the same input probe pulses as the forward transmission. Since the backward optical modes $a_{\circlearrowleft}$ and $c_{\circlearrowleft}$ decouple from the forward ones $a_{\circlearrowright}$ and $c_{\circlearrowright}$, the optical mode $a_{\circlearrowleft}$ takes a certain decay rate κ_a and an effective detuning Δ_{eff} [65]. It implies that dissipations regarding the backward transmissions only depend on the topological operation time T, irrelevant to the input eigenmodes and the direction of topological operations. Therefore, the backward transmissions in CCW and CW share the same value of $T_{mn} = -272.9$ dB for the same topological operation time, see the dashed lines in Figure 3(b and d). Here, the transmission values of T_{mn} are the ones for output pulses projected on the eigenmodes when the topological operations are finished. As probe pulses suffer from long time dissipation, the output probe pulses would be too small to be detected, and the nonreciprocal transmissions can be realized in this way.

Moreover, these final output probe pulses in Figure 3 are insensitive to the detuning δ. It is due to the fact that the final output probe pulses must be in one of the eigenmodes of the system, determined by the initial parameters of the pump field and selected by the direction of the topological operation.

As a result, our proposed synthetic $\mathcal{PT}$ symmetric optomechanics working as the topological optomechanical amplifier is feasible using current laboratory technologies [34, 63]. This optomechanical amplifier is based on the effective gain from the pump field, which opens a new way to overcome the low efficiency transmission due to the loss accumulation [49, 50, 54–56]. Compared with Ref. [34] involving a certain gain from the certain pump field, our scheme is based on a time-dependent pump field and the tunable gain enables the optical amplification with topological properties. Therefore, the accumulation of dissipations for time-dependent topological operations [56] can be overcome in this way. Moreover, our topological amplifier owns features of tunability, chirality, and topology, which are unattainable from the conventional Hermitian Hamiltonian devices [72–75]. In addition, the optical gain can be enhanced by increasing the time for topological operations via the effective gain [65], and the chirality can be switched off by increasing the topological operation time. Since the final eigenmodes in our system must be in a steady eigenmode $|\psi_-(t = T)\rangle$ when all NAT processes are finished (see Figure S3 in [65]), our system offers the possibility to observe the predicted results of a long time topological dynamics around the EP [12], which overcomes the limitation of the traditional optical gain medium [1].

5 Conclusions

We have explored how to achieve synthetic $\mathcal{PT}$ symmetry in passive optomechanics [34, 63]. In such a system, we have demonstrated that topological dynamics around the EP can be selected and manipulated by a tunable blue-detuned pump field via Stokes processes from radiation

pressure coupling, resulting in a topological amplifier. The proposed way of creating the effective optical gain via the blue-detuned pump field can be applied to diverse systems with similar processes, such as stimulated Brillouin scattering [76, 77], stimulated Raman scattering [78], and coupled nano-mechanical resonator array [79, 80]. Also, the synthetic $\mathcal{PT}$ symmetric optomechanics provides a new platform to explore time-dependent non-Hermitian dynamics [52] and topological photonics, with applications ranging from optical communications to quantum optical engineering.

Acknowledgment: J. Q. Zhang appreciates helpful discussions with Jin-Hui Wu, Xiaoming Cai and Jian Xu.

Author contribution: All the authors have accepted responsibility for the entire content of this submitted manuscript and approved submission.

Research funding: J. Q. Zhang and M. Feng are supported by Special Project for Research and Development in Key areas of Guangdong Province (Grant No. 2020B030300001), the National Key Research and Development Program of China (No. 2017YFA0304503), and the National Natural Science Foundation of China (Grant Nos. U21A20434, 91636220 and 11835011). Z. R. Gong is supported by National Natural Science Foundation of China (Grant No. 12175150) and Natural Science Foundation of Guang-dong Province (Grant No. 2019A1515011400). S. L. Su is supported by the National Natural Science Foundation of China (Grant No 11804308) H. L. Zhang and H. Jing are supported by the National Natural Science Foundation of China (Grants No. 11935006 and No. 11774086) and the Science and Technology Innovation Program of Hunan Province (Grant No. 2020RC4047).

Conflict of interest statement: The authors declare no conflicts of interest regarding this article.

References

[1] M.-A. Miri and A. Alú, "Exceptional points in optics and photonics," *Science*, vol. 363, p. 42, 2019.

[2] S. K. Özdemir, S. Rotter, F. Nori, and L. Yang, "Parity-time symmetry and exceptional points in photonics," *Nat. Mater.*, vol. 18, p. 783, 2019.

[3] El-Ganainy, K. Makris, M. Khajavikhan, Z. Musslimani, S. Rotter, and D. N. Christodoulides, "Non-Hermitian physics and PT symmetry," *Nat. Phys.*, vol. 14, p. 11, 2018.

[4] S. Klaiman, U. Gunther, and N. Moiseyev, "Visualization of branch points in $\mathcal{PT}$-symmetric waveguides symmetric optomechanics," *Phys. Rev. Lett.*, vol. 101, 2008, Art no. 080402.

[5] A. Guo, G. J. Salamo, D. Duchesne, R. Morandotti, M. Volatier-Ravat, V. Aimez, G. A. Siviloglou, and D. N. Christodoulides, "Observation of $\mathcal{PT}$-symmetry breaking in complex optical potentials," *Phys. Rev. Lett.*, vol. 103, 2009, Art no. 093902.

[6] C. E. Rüter, K. G. Makris, R. El-Ganainy, D. N. Christodoulides, M. Segev, and D. Kip, "Observation of parity-time symmetry in optics," *Nat. Phys.*, vol. 6, p. 192, 2010.

[7] L. Ge and H. E. Tureci, "Antisymmetric $\mathcal{PT}$-photonic structures with balanced positive- and negative-index materials," *Phys. Rev. A*, vol. 88, 2013, Art no. 053810.

[8] B. Peng, S. K. Özdemir, F. C. Lei, et al., "Parity-time-symmetric whispering-gallery microcavities," *Nat. Phys.*, vol. 10, p. 394, 2014.

[9] L. Chang, X. Jiang, S. Hua, et al., "Parity-time symmetry and variable optical isolation in active-passive-coupled microresonators," *Nat. Photonics*, vol. 8, p. 524, 2014.

[10] X.-Y. Lü, H. Jing, J.-Y. Ma, and Y. Wu, "$\mathcal{PT}$-symmetry-breaking chaos in optomechanics," *Phys. Rev. Lett.*, vol. 114, p. 253601, 2015.

[11] T. Gao, E. Estrecho, K. Y. Bliokh, et al., "Observation of non-Hermitian degeneracies in a chaotic exciton-polariton billiard," *Nature (London)*, vol. 526, p. 554, 2015.

[12] A. U. Hassan, B. Zhen, M. Soljacic, M. Khajavikhan, and D. N. Christodoulides, "Dynamically encircling exceptional points: exact evolution and polarization state conversion," *Phys. Rev. Lett.*, vol. 118, 2017, Art no. 093002.

[13] A. Tuniz, T. Wieduwilt, and M. A. Schmidt, "Tuning the effective PT phase of plasmonic eigenmodes," *Phys. Rev. Lett.*, vol. 123, p. 213903, 2019.

[14] Y. Wu, W. Liu, J. Geng, et al., "Observation of parity-time symmetry breaking in a single-spin system," *Science*, vol. 364, p. 878, 2019.

[15] X.-L. Zhang, T. Jiang, and C. T. Chan, "Dynamically encircling an exceptional point in anti-parity-time symmetric systems: asymmetric mode switching for symmetry-broken modes," *Light Sci. Appl.*, vol. 8, p. 88, 2019.

[16] J. Ren, H. Hodaei, G. Harari, et al., "Ultrasensitive micro-scale parity-time-symmetric ring laser gyroscope," *Opt. Lett.*, vol. 42, p. 1565, 2019.

[17] Y.-H. Lai, Y.-K. Lu, M.-G. Suh, Z. Yuan, and K. Vahala, "Observation of the exceptional-point enhanced Sagnac effect," *Nature*, vol. 576, p. 65, 2019.

[18] M. P. Hokmabadi, A. Schumer, D. N. Christodoulides, and M. Khajavikhan, "Non-Hermitian ring laser gyroscopes with enhanced sagnac sensitivity," *Nature*, vol. 576, p. 70, 2019.

[19] W. Tang, X. Jiang, K. Ding, et al., "Exceptional nexus with a hybrid topological invariant," *Science*, vol. 370, p. 1077, 2020.

[20] F. Zhang, Y. Feng, X. Chen, L. Ge, and W. Wan, "Synthetic anti-PT symmetry in a single microcavity," *Phys. Rev. Lett.*, vol. 124, 2020, Art no. 053901.

[21] H. Zhang, R. Huang, S.-D. Zhang, et al., "Breaking anti-PT symmetry by spinning a resonator," *Nano Lett.*, vol. 20, p. 7594, 2020.

[22] S. Xia, D. Kaltsas, D. Song1, et al., "Nonlinear tuning of PT symmetry and non-Hermitian topological states," *Science*, vol. 372, p. 72, 2021.

[23] C. M. Bender and S. Boettcher, "Real spectra in non-Hermitian Hamiltonians having $\mathcal{PT}$ symmetry," *Phys. Rev. Lett.*, vol. 80, p. 5243, 1998.

[24] C. M. Bender, "Making sense of non-Hermitian Hamiltonians," *Rep. Prog. Phys.*, vol. 70, p. 947, 2007.
[25] G.-Q. Zhang, Z. Chen, D. Xu, et al., "Exceptional point and cross-relaxation effect in a hybrid quantum system," *PRX Quantum*, vol. 2, 2021, Art no. 020307.
[26] W. Xiong, Z. Li, Y. Song, J. Chen, G.-Q. Zhang, and M. Wang, "Higher-order exceptional point in a pseudo-Hermitian cavity optomechanical system," *Rep. Prog. Phys.*, vol. 70, p. 947, 2007.
[27] J. Wiersig, "Enhancing the sensitivity of frequency and energy splitting detection by using exceptional points: application to microcavity sensors for single-particle detection," *Phys. Rev. Lett.*, vol. 112, p. 203901, 2014.
[28] Z.-P. Liu, J. Zhang, S. K. Özdemir, B. Peng, H. Jing, X.-Y. Lü, C.-W. Li, L. Yang, F. Nori, and Y.-x. Liu, "Metrology with $\mathcal{PT}$-symmetric cavities: enhanced sensitivity near the $\mathcal{PT}$-phase transition," *Phys. Rev. Lett.*, vol. 117, p. 110802, 2016.
[29] H. Hodaei, A. U. Hassan, S. Wittek, et al., "Enhanced sensitivity at higher-order exceptional points," *Nature (London)*, vol. 548, p. 187, 2017.
[30] W. Chen, S. K. Özdemir, G. Zhao, J. Wiersig, and L. Yang, "Exceptional points enhance sensing in an optical microcavity," *Nature*, vol. 548, p. 192, 2017.
[31] L. Feng, Z. J. Wong, R.-M. Ma, Y. Wang, and X. Zhang, "Single-mode laser by parity-time symmetry breaking," *Science*, vol. 346, p. 972, 2014.
[32] H. Hodaei, M.-A. Miri, M. Heinrich, D. N. Christodoulides, and M. Khajavikhan, "Parity-time symmetric microring lasers," *Science*, vol. 346, p. 975, 2014.
[33] H. Jing, S. K. Özdemir, X.-Y. Lü, J. Zhang, L. Yang, and F. Nori, "$\mathcal{PT}$-Symmetric phonon laser," *Phys. Rev. Lett.*, vol. 113, 2014, Art no. 053604.
[34] J. Zhang, B. Peng, S. K. Özdemir, et al., "A phonon laser operating at an exceptional point," *Nat. Photonics*, vol. 12, p. 479, 2018.
[35] H. Zhang, F. Saif, Y. Jiao, and H. Jing, "Loss-induced transparency in optomechanics," *Opt. Express*, vol. 19, p. 25199, 2018.
[36] B. Peng, S. K. Özdemir, S. Rotter, et al., "Loss-induced suppression and revival of lasing," *Science*, vol. 346, p. 328, 2014.
[37] S. Assawaworrarit, X. Yu, and S. Fan, "Robust wireless power transfer using a nonlinear parity-time-SymmetricCircuit," *Nature (London)*, vol. 546, p. 387, 2017.
[38] J. Song, F. Yang, Z. Guo, et al., "Wireless power transfer via topological modes in dimer chains," *Phys. Rev. Appl.*, vol. 15, 2021, Art no. 014009.
[39] K. Kawabata, K. Shiozaki, M. Ueda, and M. Sato, "Symmetry and topology in non-Hermitian physics," *Phys. Rev. X*, vol. 9, 2019, Art no. 041015.
[40] H. Zhou and J. Y. Lee, "Periodic table for topological bands with non-Hermitian symmetries," *Phys. Rev. B*, vol. 99, p. 235112, 2019.
[41] F. K. Kunst, E. Edvardsson, J. C. Budich, and E. J. Bergholtz, "Biorthogonal bulk-boundary correspondence in non-Hermitian systems," *Phys. Rev. Lett.*, vol. 121, 2018, Art no. 026808.
[42] S. Yao and Z. Wang, "Edge states and topological invariants of non-Hermitian systems," *Phys. Rev. Lett.*, vol. 121, 2018, Art no. 086803.
[43] E. J. Bergholtz, J. C. Budich, and F. K. Kunst, "Exceptional topology of non-Hermitian systems," *Rev. Mod. Phys.*, vol. 93, 2021, Art no. 015005.
[44] T. E. Lee, "Anomalous edge state in a non-Hermitian lattice," *Phys. Rev. Lett.*, vol. 116, p. 133903, 2016.
[45] L. Xiao, T. Deng, K. Wang, et al., "Non-Hermitian bulk-boundary correspondence in quantum dynamics," *Nat. Phys.*, vol. 16, p. 761, 2020.
[46] K. Zhang, Z. Yang, and C. Fang, "Correspondence between winding numbers and skin modes in non-Hermitian systems," *Phys. Rev. Lett.*, vol. 125, p. 126402, 2020.
[47] H. Xu, D. Mason, L. Jiang, and J. G. E. Harris, "Topological energy transfer in an optomechanical system with exceptional points," *Nature*, vol. 537, p. 80, 2016.
[48] Y. Choi, C. Hahn, J. W. Yoon, S. H. Song, and P. Berini, "Extremely broadband, on-chip optical nonreciprocity enabled by mimicking nonlinear anti-adiabatic quantum jumps near exceptional points," *Nat. Commun.*, vol. 8, p. 14154, 2017.
[49] J. Doppler, A. A. Mailybaev, P. Rabl, N. Moiseyev, and S. Rotter, "Dynamically encircling an exceptional point for asymmetric mode switching," *Nature (London)*, vol. 537, p. 76, 2016.
[50] X.-L. Zhang, S. Wang, B. Hou, and C. T. Chan, "Dynamically encircling exceptional points: in situ control of encircling loops and the role of the starting point," *Phys. Rev. X*, vol. 8, 2018, Art no. 021066.
[51] C. Dembowski, H.-D. Grüf, H. L. Harney, et al., "Experimental observation of the topological structure of exceptional points," *Phys. Rev. Lett.*, vol. 86, p. 787, 2001.
[52] W. Liu, Y. Wu, C.-K. Duan, X. Rong, and J. Du, "Dynamically encircling an exceptional point in a real quantum system," *Phys. Rev. Lett.*, vol. 126, p. 170506, 2021.
[53] H. Zhou, J. Y. Lee, S. Liu, and B. Zhen, "Exceptional surfaces in PT-symmetric non-Hermitian photonic systems," *Optica*, vol. 6, p. 190, 2019.
[54] Q. Liu, S. Li, B. Wang, et al., "Efficient mode transfer on a compact silicon chip by encircling moving exceptional points," *Phys. Rev. Lett.*, vol. 124, p. 153903, 2020.
[55] A. Li, J. Dong, J. Wang, et al., "Hamiltonian hopping for efficient chiral mode switching in encircling exceptional points," *Phys. Rev. Lett.*, vol. 125, p. 187403, 2020.
[56] J. W. Yoon, Y. Choi, C. Hahn, et al., "Time-asymmetric loop around an exceptional point over the full optical communications band," *Nature (London)*, vol. 562, p. 86, 2018.
[57] M. Aspelmeyer, P. Meystre, and K. Schwab, "Quantum optomechanics," *Phys. Today*, vol. 65, p. 29, 2012.
[58] P. Meystre, "A short walk through quantum optomechanics," *Ann. Phys.*, vol. 525, p. 215, 2013.
[59] W. Nie, M. Antezza, Y.-X. Liu, and F. Nori, "Dissipative topological phase transition with strong system-environment coupling," *Phys. Rev. Lett.*, vol. 127, p. 250402, 2021.
[60] T. Liu, J. J. He, Z. Yang, and F. Nori, "Higher-order Weyl-exceptional-ring semimetals," *Phys. Rev. Lett.*, vol. 127, p. 196801, 2021.

[61] C. Gneiting, A. Koottandavida, A. V. Rozhkov, and F. Nori, "Unraveling the topology of dissipative quantum systems," arXiv:2007.05960, 2020.
[62] M. Aspelmeyer, T. J. Kippenberg, and F. Marquardt, "Cavity optomechanics," *Rev. Mod. Phys.*, vol. 86, p. 1391, 2014.
[63] I. S. Grudinin, H. Lee, O. Painter, and K. J. Vahala, "Phonon laser action in a tunable two-level system," *Phys. Rev. Lett.*, vol. 104, 2010, Art no. 083901.
[64] F. Ruesink, M.-A. Miri, A. Alù, and E. Verhagen, "Nonreciprocity and magnetic-free isolation based on optomechanical interactions," *Nat. Commun.*, vol. 7, p. 136602, 2016.
[65] See Supplemental Material for details. (a) Derivation of mean value equation (3), see S1. (b) Derivation of Hamiltonian (6), see S2. (c) Derivation of the long time topological dynamical steady state, see S3. (d) The parameter relations for Figure 2, see S4. (e) Simulations for topological dynamical steady results, see S5. (f) The switchable chirality of topological optomechanical amplification, see S6, Figure S5 and Figure S6. (g) Populations of topological energy transfer, see S7. (h) Supplemental figures regarding Figures 2 and 3.
[66] D. F. Walls and G. J. Milburn, *Quantum Optics*, Berlin, Springer-Verlag, 1994.
[67] T. J. Milburn, J. Doppler, C. A. Holmes, S. Portolan, S. Rotter, and P. Rabl, "General description of quasiadiabatic dynamical phenomena near exceptional points," *Phys. Rev. A*, vol. 92, 2015, Art no. 052124.
[68] S. Weis, R. Rivière, S. Deléglise, et al., "Optomechanically induced transparency," *Science*, vol. 330, p. 1520, 2010.
[69] L. Feng, Y.-L. Xu, W. S. Fegadolli, et al., "Experimental demonstration of a unidirectional reflectionless parity-time metamaterial at optical frequencies," *Nat. Mater.*, vol. 12, p. 108, 2012.
[70] H. Shen, B. Zhen, and L. Fu, "Topological band theory for non-Hermitian Hamiltonians," *Phys. Rev. Lett.*, vol. 120, p. 146402, 2018.
[71] K. Kawabata, T. Bessho, and M. Sato, "Classification of exceptional points and non-Hermitian topological semimetals," *Phys. Rev. Lett.*, vol. 123, 2019, Art no. 066405.
[72] F. Yang, F. Gyger, and L. Thevenaz, "Intense Brillouin amplification in gas using hollow-core waveguides," *Nat. Photonics*, vol. 14, p. 700, 2020.
[73] Z. Shen, Y.-L. Zhang, Y. Chen, et al., "Experimental realization of optomechanically induced non-reciprocity," *Nat. Photonics*, vol. 10, p. 657, 2016.
[74] Z. Shen, Y.-L. Zhang, Y. Chen, et al., "Reconfigurable optomechanical circulator and directional amplifier," *Nat. Commun.*, vol. 9, p. 1797, 2018.
[75] D. Malz, L. D. Tóth, N. R. Bernier, A. K. Feofanov, T. J. Kippenberg, and A. Nunnenkamp, "Quantum-limited directional amplifiers with optomechanics," *Phys. Rev. Lett.*, vol. 120, 2018, Art no. 023601.
[76] J. Kim, M. C. Kuzyk, K. Han, H. Wang, and G. Bahl, "Non-reciprocal Brillouin scattering induced transparency," *Nat. Phys.*, vol. 11, p. 275, 2015.
[77] C.-H. Dong, Z. Shen, C.-L. Zou, Y.-L. Zhang, W. Fu, and G.-C. Guo, "Brillouin-scattering-induced transparency and non-reciprocal light storage," *Nat. Commun.*, vol. 6, p. 6193, 2015.
[78] G. P. Agrawal, *Nonliner Fiber Optics*, Berlin, Heidelberg, Springer, 2000.
[79] H. Okamoto, A. Gourgout, C. Y. Chang, et al., "Coherent phonon manipulation in coupled mechanical resonators," *Nat. Phys.*, vol. 9, p. 480, 2013.
[80] I. Mahboob, H. Okamoto, and H. Yamaguchi, "An electromechanical Ising Hamiltonian," *Sci. Adv.*, vol. 2, 2016, Art no. e1600236.

Supplementary Material: The online version of this article offers supplementary material (https://doi.org/10.1515/nanoph-2021-0721).